Chapter 7 – Evolution of the active volume in irradiated detectors

7.1 Charge collection from low range particle illumination

The low range particles used were α particles from a ^{241}Am source and low energy protons from the Prague Van de Graaf accelerator [6.1]. α's from the americium source have energies of 5.49 MeV (85%) and 5.44 MeV (13%). The Van de Graaf accelerator provides a proton current with energies up to 2.5 MeV. The set-ups for the charge collection measurements with α particles and Van de Graaf protons are described in Appendix A.

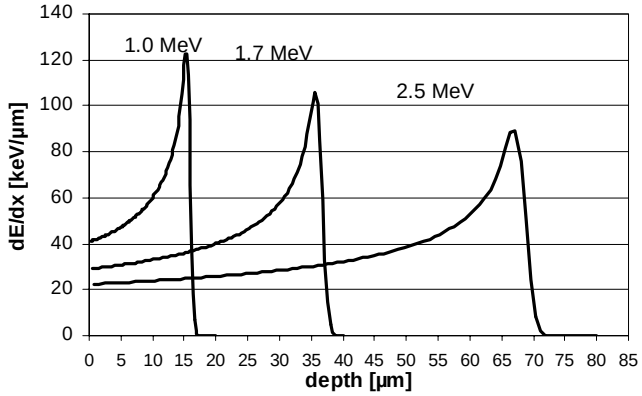

Fig. 7.1 *Simulated specific energy loss of low-range protons in silicon.*

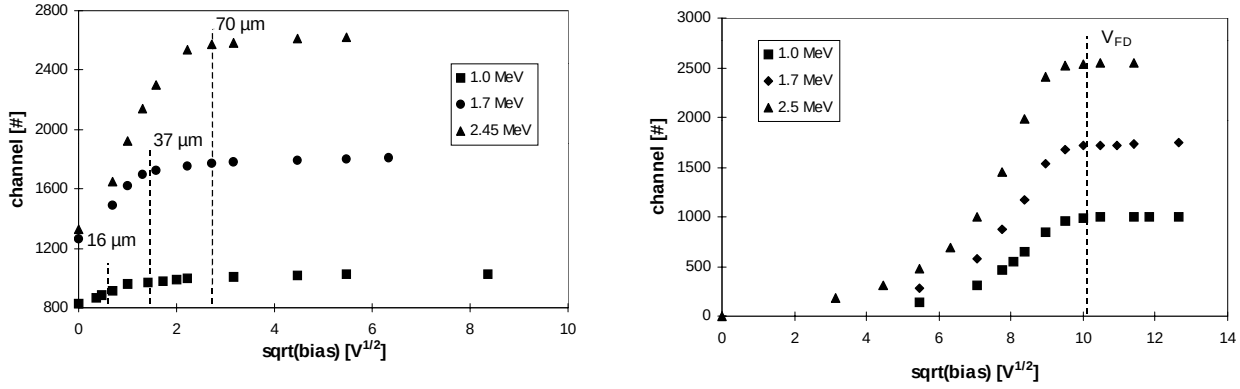

(a) (b)

Fig. 7.2 *Charge collection versus $V^{1/2}$, recorded by an ADC, for (a) front and (b) rear illumination of a non-irradiated silicon detector with protons of different energies.*

Charge collection for non-irradiated diodes.

Figure 7.1 shows the specific energy loss for 1, 1.7 and 2.5 MeV protons in silicon. Figure 7.2 shows the charge collection as a function of $V^{1/2}$ for a non-irradiated diode illuminated by 1, 1.7 and 2.5 MeV protons from the Van de Graaf accelerator, in the case of front injection (a) or rear injection (b).

For front injection, 100% of the charge is collected when the depletion depth, x_d, is equal or larger than the range x_R of the particle in silicon, as it can be noticed comparing figure 7.1 and 7.2(a). Calling V_R the voltage corresponding to the depletion depth x_R, the total charge collection takes place for $V \geq V_R$.

When the particles are injected through the ohmic side, the model predicts no charge collection up to the voltage, V'_R, corresponding to a depletion depth of $w - x_R$, where w is the detector thickness. 100% of the charge is collected at full depletion, independently on the energy of the impinging particle.

However, the charge collection is enhanced, for bias voltages below V_{FD}, due to the diffusion of carriers through the non-depleted bulk, when the integration time of the charge amplifier is long enough (0.5 µs) to get part of this diffusing charge.

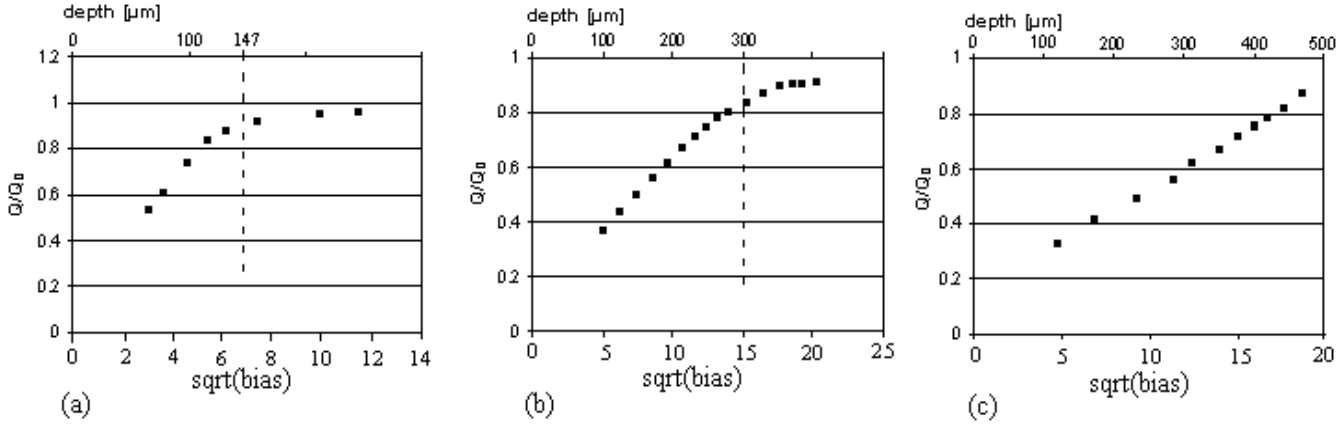

Fig. 7.3 *CCE as a function of $V^{1/2}$ for diodes of different thicknesses irradiated by protons to ≈ 7.5 10^{13} cm^{-2}. The α source was positioned on the rear side. Diode thicknesses: (a) 147µm, (b) 303µm, (c) 503µm.*

Charge collection for irradiated diodes.

Figure 7.3 shows the CCE as a function of $V^{1/2}$ for signals induced by α particle from a ^{241}Am source for similarly irradiated detectors (≈ $7.5 \cdot 10^{13}$ 24 GeV/c protons cm^{-2}, above type inversion) of different thickness. The particles were impinging on the rear side of the detector, corresponding to the junction side after inversion. The measurements were performed in air atmosphere and the distance between the α source and the detector was ≈ 1 cm. The energy of the α particles entering the detectors was ≈ 4.5 MeV and the range of the particle in silicon ≈ 25 µm. The charge collection curve is normalised to the maximum charge collected before irradiation, Q_0. All the diodes collect about 90% of Q_0 at bias voltages larger than V_{FD} but the charge collected at any arbitrary depletion depth for $V < V_{FD}$ is different. The 150 µm thick diode collects, at $V = V_{FD}$, (V_{FD} was estimated by C-V measurement), ≈ 85% of Q_0. For the 300 µm and the 500 µm thick diodes, the charge collected at the depletion depth of 150 µm is 55% and < 40% respectively. This result indicates a dependence of the charge collection on the non-depleted part of the detector. The collected charge, as a function of bias below V_{FD} is [7.1]:

$$Q(V) = \frac{Q_0 x_d}{w} = Q_0 \sqrt{\frac{V}{V_{FD}}} \tag{7.1}$$

The moving charge carriers induce a signal on the electrodes of the detector until they reach the boundary of the depleted bulk. The collected charge is the integral of the induced current from the injection time to the end of the carrier motion. This interval of time is defined as the collection time, t_c. For irradiated diodes, t_c is independent on the applied reverse bias up to full depletion. t_c can be expressed as follows:

$$t_c = \frac{x_d}{v_{average}} = \frac{x_d}{\frac{1}{x_d}\int_0^{x_d} \mu E(x)dx} = \frac{x_d}{-\frac{1}{x_d}\int_0^{x_d} \mu \frac{dV(x)}{dx}} = \frac{x_d^2}{\mu V_{bias}} = \frac{2\varepsilon_{Si}}{q\mu N_{eff}} \tag{7.2}$$

where x_d is the drift distance and the mobility μ is considered to be constant. The assumption of the mobility as independent on the bias is reasonable, because the saturation of the mobility at high electric field is expected for bias voltages higher than V_{FD}. It is opportune to notice that the trapping effect on carriers is independent on the bias below full depletion. The effect of trapping on the collected charge is expressed by :

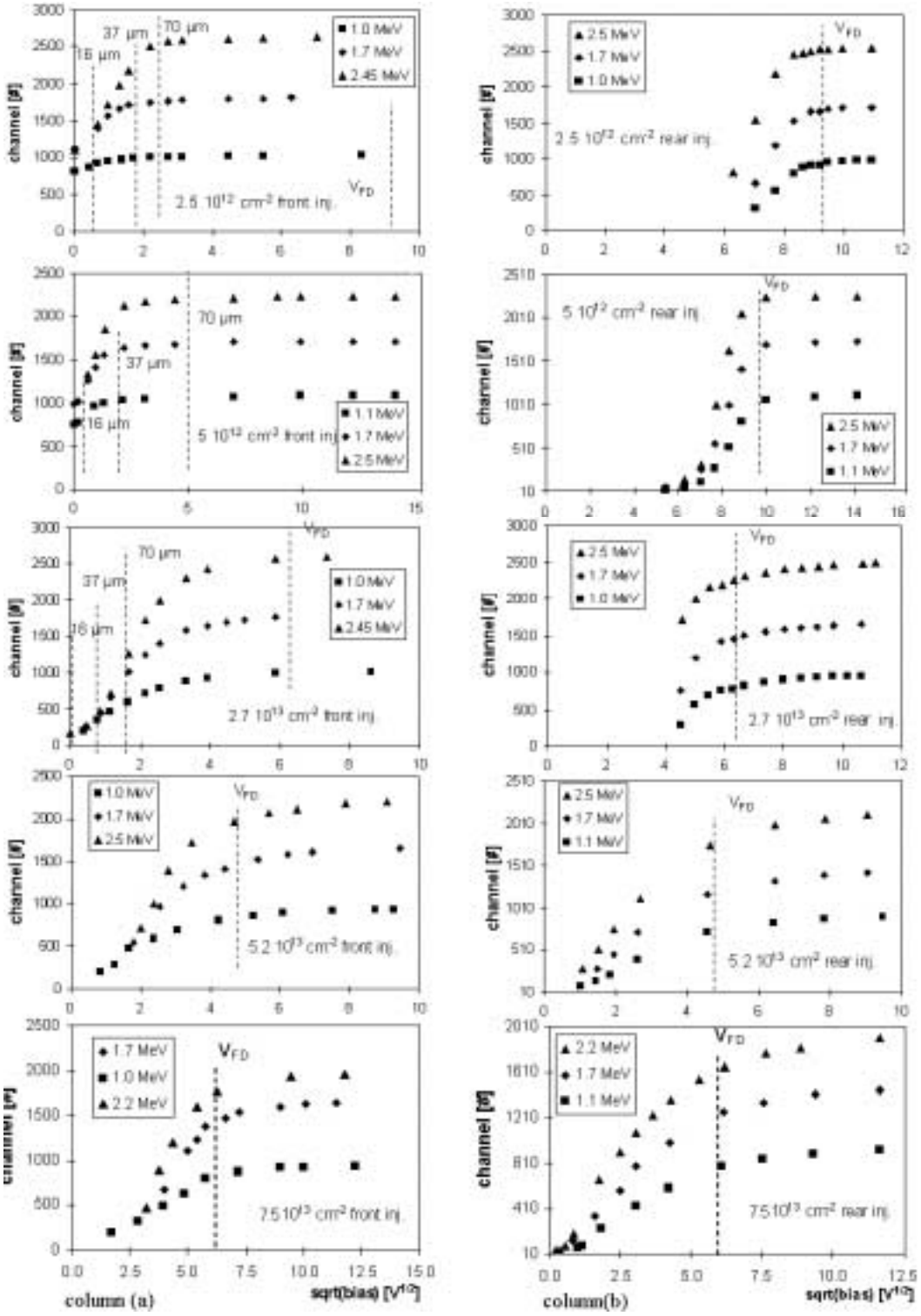

Fig. 7.4 *Charge collection (CC) versus $V^{1/2}$ for variously irradiated diodes illuminated by protons of different energies from a Van de Graaf accelerator [6.1]. The CC is recorded by an ADC in the case of front injection (column (a)) and rear injection (column (b)).*

$$Q(t) = Q_0 e^{-\frac{t_c}{\tau_{tr}}} \tag{7.3}$$

where τ_{tr} is the charge carrier lifetime [3.20]. The reduction in the charge collection below V_{FD} due to the trapping effect is constant, because of the independence of t_c on $V^{1/2}$ up to full depletion. The expression of the charge collected for bias voltages below full depletion should be corrected by:

$$Q(V) = \frac{Q_0 x_d}{w} e^{-\frac{t_c}{\tau_{tr}}} = Q_0 e^{-\frac{t_c}{\tau_{tr}}} \sqrt{\frac{V}{V_{FD}}} \tag{7.4}$$

Above V_{FD}, the drift distance coincides with the detector thickness while the velocity increases with the bias (until saturation). The subsequent reduction of t_c results in an improvement of the charge collection above V_{FD} according to eq. 7.3.

Figure 7.4 shows the charge collection as a function of bias for variously irradiated diodes (from $2.5 \cdot 10^{12}$ to $5.7 \cdot 10^{13}$ cm^{-2}) illuminated by protons of different energies (from 1.0 to 2.5 MeV) in the case of front (column (a)) and rear (column (b)) illumination [7.2]. The inversion fluence for these planar 280 µm thick diodes was about $5 \cdot 10^{13}$ cm^{-2}. The differences between the behaviour of non-irradiated and irradiated diodes is evident for fluences > $5 \cdot 10^{12}$ cm^{-2}, when the complete charge collection takes place at bias voltages larger than V_R.

The CCE behaviours of irradiated and non-irradiated devices are different also when the particles impinge the detector in the side opposite to the junction. The junction is on the front side up to $5 \cdot 10^{13}$ cm^{-2} and on the rear side at higher fluences.

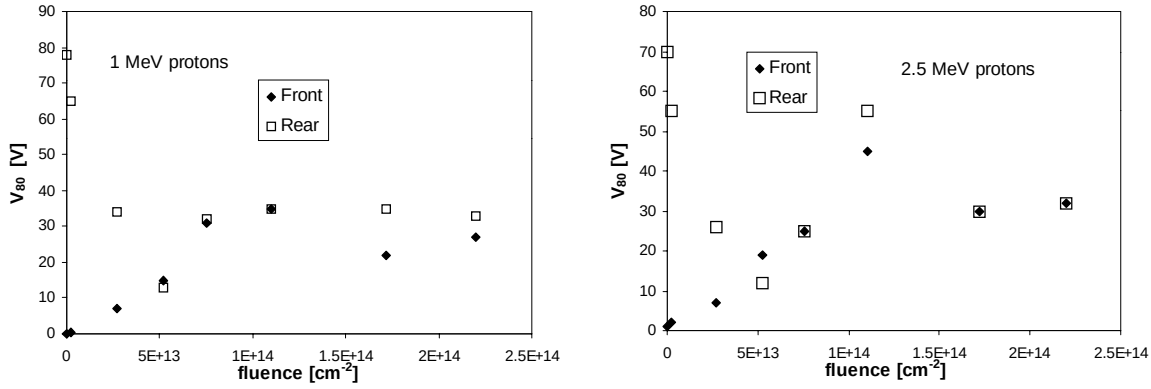

Fig. 7.5 *V_{80} as a function of fluence for front and rear injection of low range protons: (a) 1 MeV (b) 2.5 MeV protons.*

The charge collection of inverted diodes starts at bias voltages appreciably lower than V_{FD}, in the case of injection through both sides. Figure 7.5 shows V_{80} as a function of fluence, where V_{80} is the bias voltage at which 80% of the maximum charge is collected. V_{80} was chosen to minimise the error. A natural choice would be the bias at which there is a maximum charge collection (V_M). As pointed out previously, the trapping effect makes the charge collection increasing after full depletion and the definition of V_M is affected by a large error. The charge collection curve increases steeper below full depletion and the choice of V_{80} allows the reduction of the error of the estimate.

After the inversion fluence, V_{80} is similar in case of injection from both sides, showing that an important charge collection takes place in both sides of the detector below V_{FD}. This suggests the presence of a sensitive region close to the ohmic contact in irradiated detectors. The definition of ohmic contact is used here to identify the contact opposite to the junction. In fact, the results presented here highlight that this definition is not correct for irradiated devices. The following sections discuss this point with more details, proposing a model for the electric field distribution next to both contacts.

7.2 Charge collection from red LED light illumination

Red light (670 nm) pulses from a light emitting diode (LED) are used to produce shallow electron or hole injection. The availability of an external trigger and the high injection level makes this source particularly convenient. The strong injection provides a high signal-over-noise ratio and the external trigger allows the study of the small pulses at low electric field that are lost with the self-trigger mode used with low range particles.

The study was carried out using a fast current amplifier and a 300 MHz band-pass digital oscilloscope (Lecroy 9361) with a 2.5 Gs/s-sampling (see Appendix A). The light injection was performed using the LED driven by an external pulse generator that also provided the trigger to the scope for recording the pulses. The FWHM of the LED pulse is ≈ 15 ns as shown by Fig.7.6. The signal pulse shape and the integral of the signal with time were recorded with the oscilloscope, after averaging over ≈ 400 triggers. The charge collection efficiency (CCE) as a function of the bias is normalised to the maximum value Q_M, defined as the averaged value of

the charge collected over a few points above the full depletion voltage (V_{FD}). This normalisation allows a better comparison between the CCE curves for detectors irradiated to different fluences. Table 7.1 lists the diodes used for this study and their respective irradiation fluences.

Detector name	Fluence [cm^{-2}]	Detector name	Fluence [cm^{-2}]	Detector name	Fluence [cm^{-2}]
P189-S-A1-18	Non irradiated	P12-S-A3-11	$5.2 \cdot 10^{13}$	P88-S-A1-17	$2.9 \cdot 10^{14}$
T3P-C-A3-3	Non irr. p-type	P88-S-A1-19	$1 \cdot 10^{14}$	P189-S-A1-21	$2.9 \cdot 10^{14}$
P189-S-A1-17	$1 \cdot 10^{12}$	P189-S-A1-22	$1 \cdot 10^{14}$		
P88-S-A1-14	$1.5 \cdot 10^{13}$	P12-S-A3-16	$1.7 \cdot 10^{14}$		

Table 7.1 *Detectors used for the LED charge collection study. The detectors are 280 µm thick silicon diodes made from standard FZ silicon and irradiated with 24 GeV/c protons. All the diodes are n-type, unless otherwise indicated.*

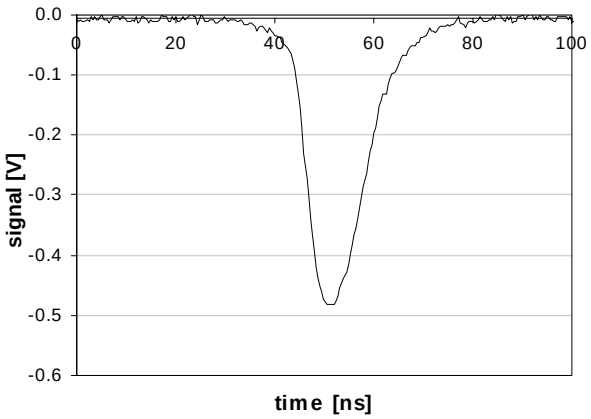

Fig. 7.6 *Shape of the LED pulse measured with a PM.*

Figure 7.7 shows the CCE curves for non-irradiated n and p-type diodes, for front and rear illumination. When the charge is injected through the front contact, there is almost complete charge collection already without any external reverse bias, due to the depleted region created by the built-in voltage. In this situation, the electric field is low and the collection time is long. Figure 7.8(a) shows the pulse shapes for front injection in a non-irradiated n-type diode, and the collection time at 0 bias voltage is > 200 ns. When an external reverse bias is applied, the collection time is faster due to the increased velocity of the moving charge, proportional to the

strength of the electric field. The peaking time, t_p, of the signal is ≈ 12 ns (peak position minus trigger time) and it is only slightly, or not at all, influenced by increasing the bias (Fig. 7.9). The independence of t_p on the reverse bias indicates that the carriers are moving in a decreasing

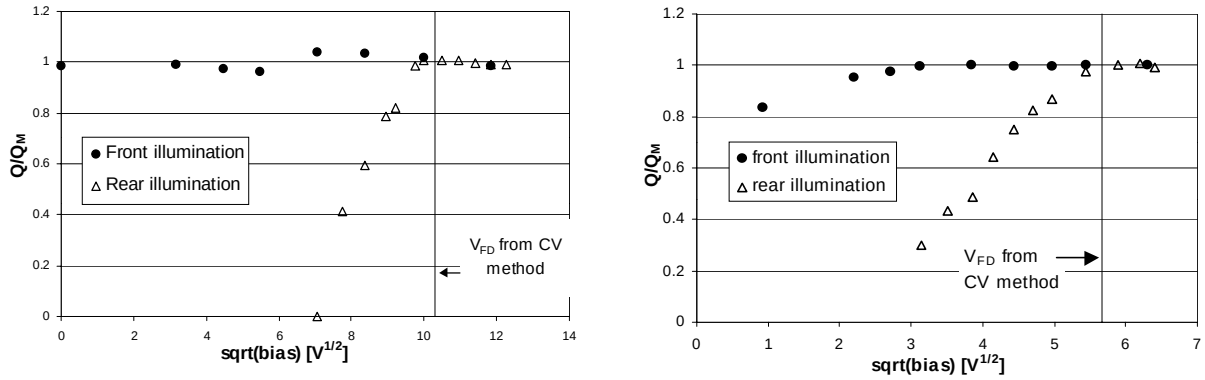

(a) (b)

Fig 7.7 *CCE as a function of $V^{1/2}$ for front and rear illumination of non-irradiated (a) n-type and (b) p-type diodes.*

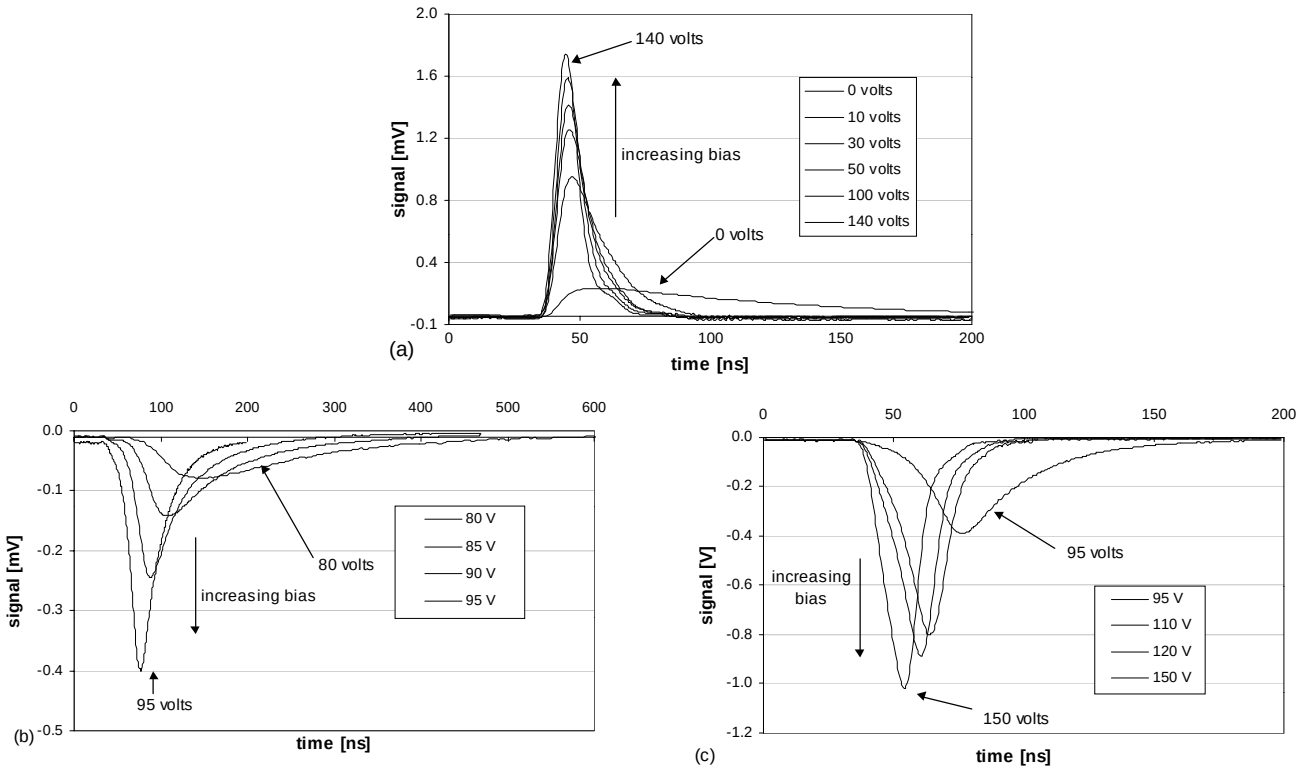

Fig. 7.8 *Signal pulse shape in a non-irradiated n-type diode. (a) Front illumination (b) Rear illumination from 80 to 95 volts (c) Rear illumination from 95 to 150 volts. V_{FD} = 105 volts.*

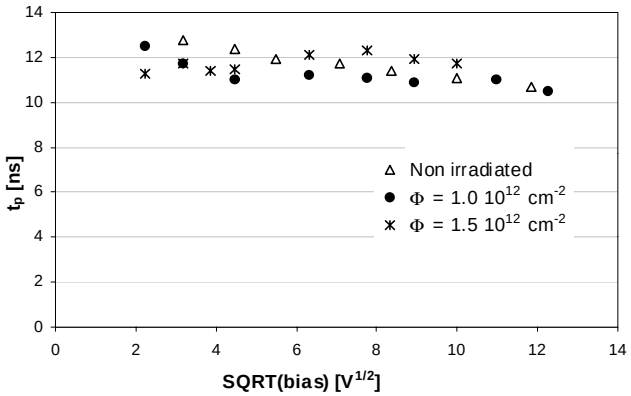

Fig. 7.9 *Peaking time versus $V^{1/2}$ for a non-irradiated and irradiated (low fluences) diodes for front LED illumination.*

electric field. When the LED illuminates the rear side of non-depleted detector, the charge is generated in a non-sensitive region and no current pulse is induced on the diode electrodes. The pulse should appear when the depletion region, developing from the junction (front) side, reaches the layer where the charge is deposited. However, the CCE curves for the rear illumination of a non-irradiated n-type and p-type diodes (Fig. 7.7) show a partial charge collection well before the full depletion is achieved. The total collection time is large compared to the collection time of the charge carriers produced in the electric field region, as it can be seen from the pulse shapes shown by Fig. 7.8(b) and (c). It is possible to evaluate the carrier velocity in the QNB. The signal is due to the charge diffusing from the non-depleted bulk (quasi-neutral bulk, QNB) towards the depleted region (space charger region, SCR). The peaking time of the pulse, t_p, is the sum of the time (t_{tr}) spent by the carriers to cross the QNB before to be injected into the field region, and the time to traverse the SCR. This time coincides with the collection time of the carriers and it is constant (t_{FD}) up to the full depletion of the diode (eq. 7.2).

The expression for t_p is:

$$t_p(V) = t_{FD} + t_{tr}(V) = t_{FD} + \frac{\Delta x}{v_{un}} = t_{FD} + \frac{w}{v_{un}}\left(1 - \sqrt{\frac{V}{V_{FD}}}\right) \qquad (7.6)$$

where v_{un} is the average velocity of the carriers in the QNB. Figure 7.10 shows $t_p(V)$ as a function of $(V/V_{FD})^{1/2}$ for non-irradiated p-type and n-type diodes illuminated through the rear side. The signal for the n-type diode is due to holes. Inversely, the signal for the n-type diode is due to electrons. For bias voltages far from V_{FD}, the values of t_p are well aligned on a straight

line. The velocity in the non-depleted bulk calculated by fitting the data with eq. 7.6 is $1.0 \cdot 10^4$ cm s^{-1} for holes and $1.5 \cdot 10^4$ cm s^{-1} for electrons.

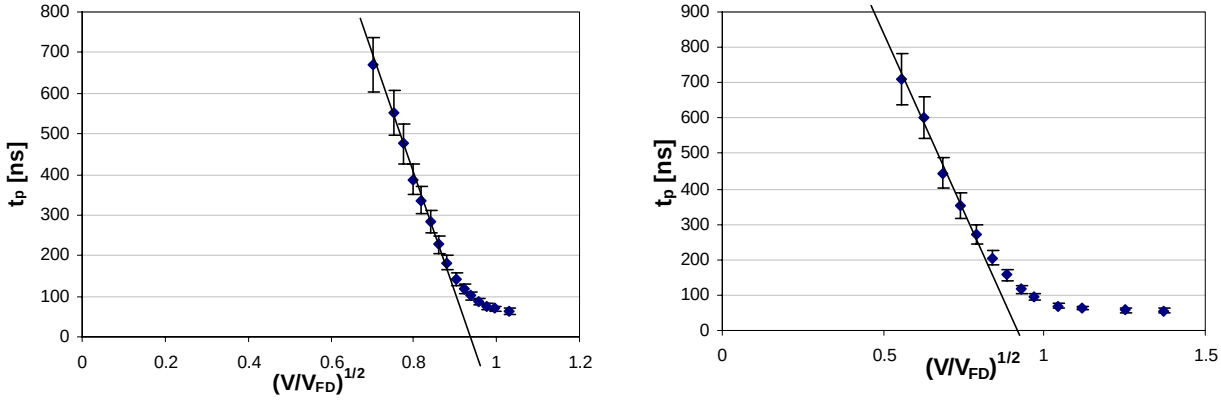

Fig. 7.10 *Peaking time (t_p) versus $(V/V_{FD})^{1/2}$ for rear injection in (a) n-type and (b) p-type non irradiated diodes.*

Red LED light in irradiated diodes

Figure 7.11 shows the CCE versus $V^{1/2}$ for detectors irradiated below the type inversion fluence. The detector irradiated up to $1.2 \cdot 10^{12}$ cm^{-2} exhibits charge collection properties similar to the non-irradiated diodes. The diode irradiated up to $1.5 \cdot 10^{13}$ cm^{-2} exhibits a linear dependence to $V^{1/2}$ for illumination through the junction (front) side.

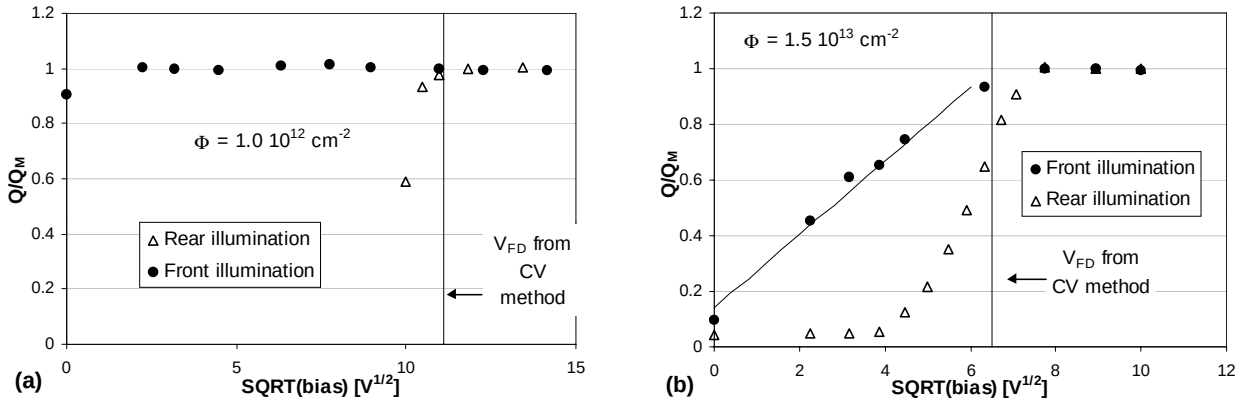

Fig 7.11 *CCE versus $V^{1/2}$ for front and rear illumination of n-type irradiated (non-inverted) diodes: (a) $\Phi = 1.0 \cdot 10^{12}$ cm^{-2} ($\Phi < \Phi_{inv}$), (b) $\Phi = 1.5 \cdot 10^{13}$ cm^{-2} ($\Phi < \Phi_{inv}$).*

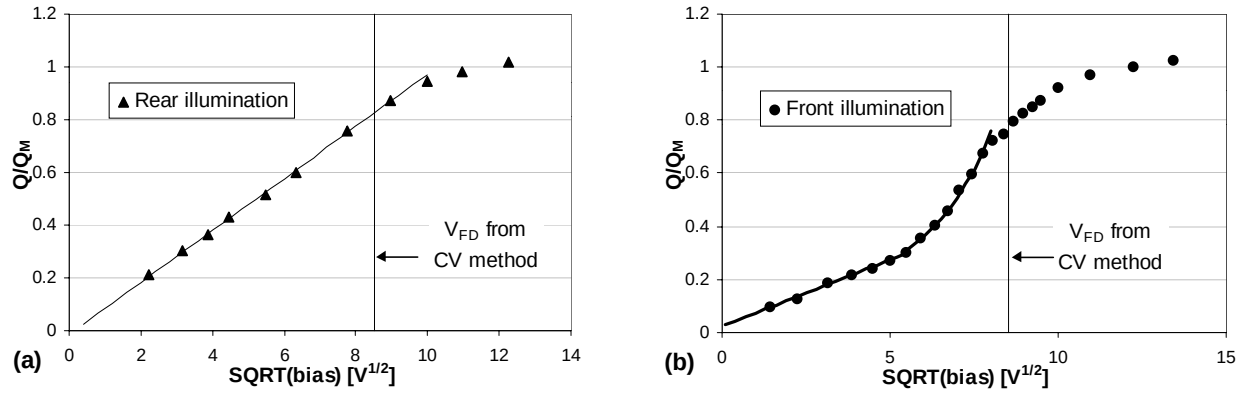

Fig 7.12 *CCE versus $V^{1/2}$ for an n-type diode irradiated up to $\Phi = 1.0 \cdot 10^{14}$ cm^{-2} ($\Phi > \Phi_{inv}$). (a) rear illumination (b) front illumination.*

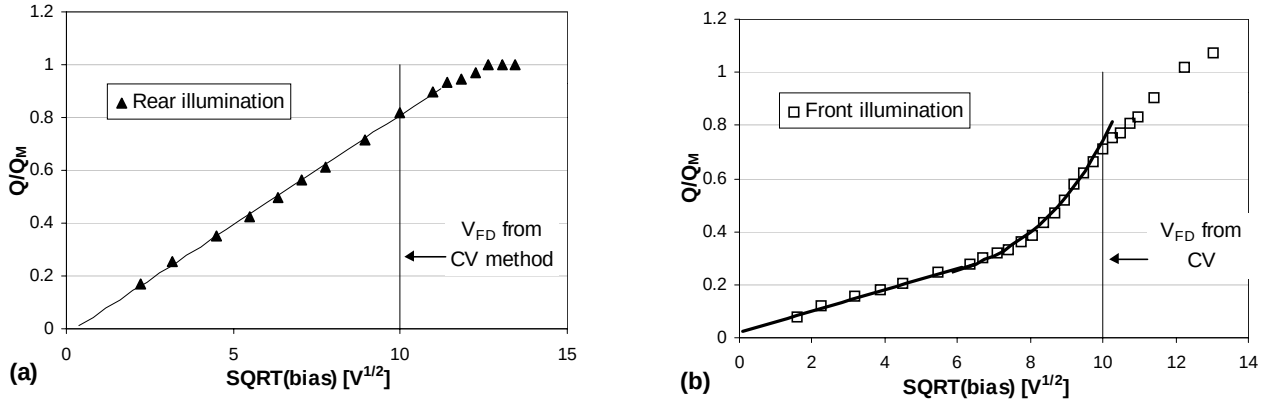

Fig 7.13 *CCE versus $V^{1/2}$ for an n-type diode irradiated up to $\Phi = 1.7 \cdot 10^{14}$ cm^{-2} ($\Phi > \Phi_{in}$). (a) rear illumination (b) front illumination.*

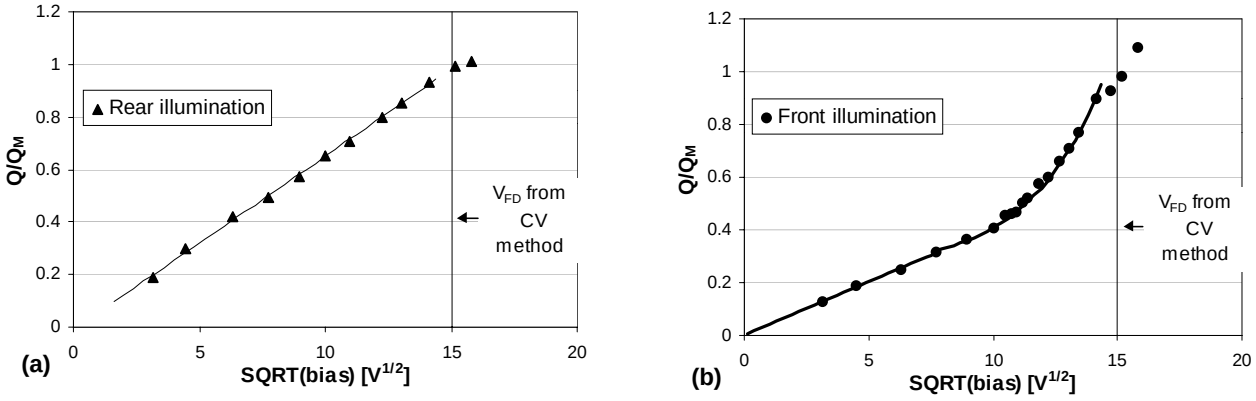

Fig 7.14 *CCE versus $V^{1/2}$ for an n-type diode irradiated up to $\Phi = 2.9 \cdot 10^{14}$ cm^{-2} ($\Phi > \Phi_{inv}$). (a) rear illumination (b) front illumination.*

For detectors irradiated above the type inversion fluence, the CCE's are proportional to the square root of bias when the light illuminates the rear side of the detectors, as shown by Fig. 7.12(a), 7.13(a) and 7.14(a). This confirms that the main junction has moved from the front to the rear side.

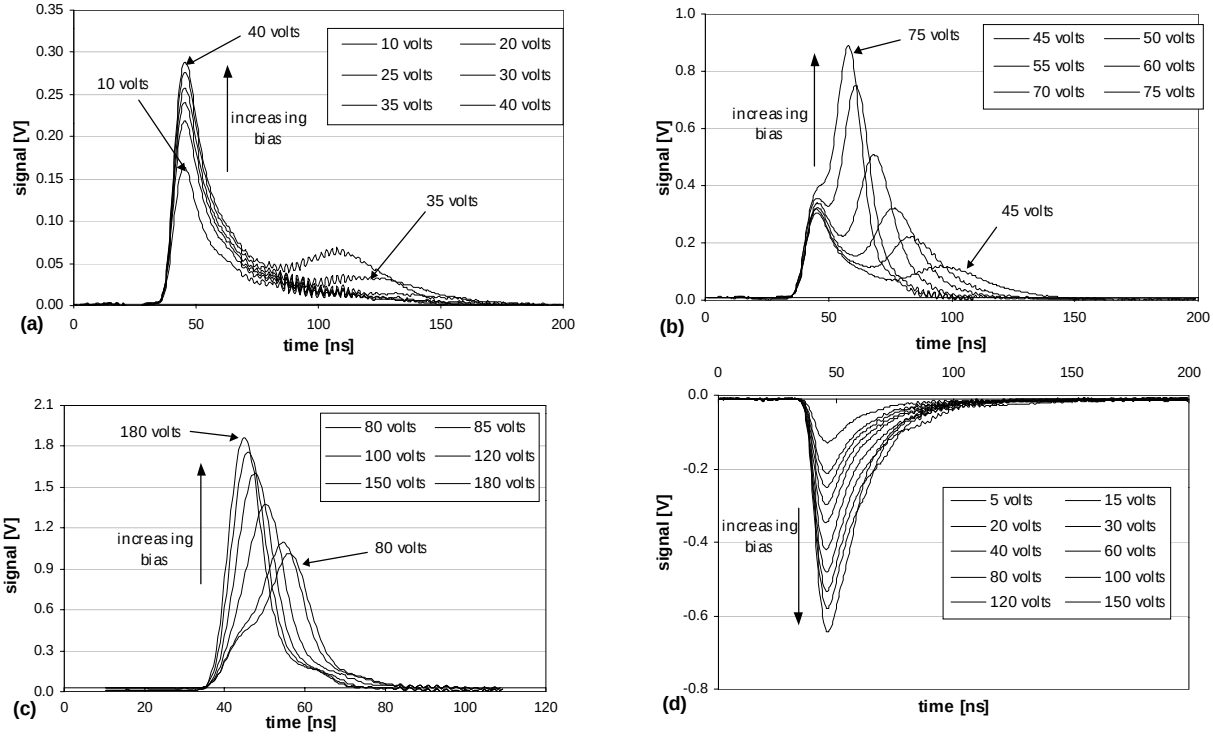

Fig. 7.15 *Signal pulses for $1 \cdot 10^{14}$ cm^{-2} irradiated diode illuminated by red LED light.*
(a) Front illumination: 10-40 V (b) Front illumination: 45-75 V
(c) Front illumination: 80-180 V (d) Rear illumination 5-150 V. V_{FD} = 70 volts.

The analysis of the pulse shapes for inverted diodes as a function of bias also confirms the presence of the junction at the rear side of the detector. When the light illuminates the rear side (Fig. 7.15(d), 7.16(d) and 7.17(d)), the signal is visible from low bias voltages, as expected from the injection in the electric field region. The peaking time is ≈ 14 ns and does not change with increasing bias, indicating that the holes drift towards the cathode in the direction of decreasing electric field. Figure 7.18 shows the peak height (p_H) as a function of $V^{1/2}$. p_H is proportional to the current at the injection time ($t = 0$), which can be written:

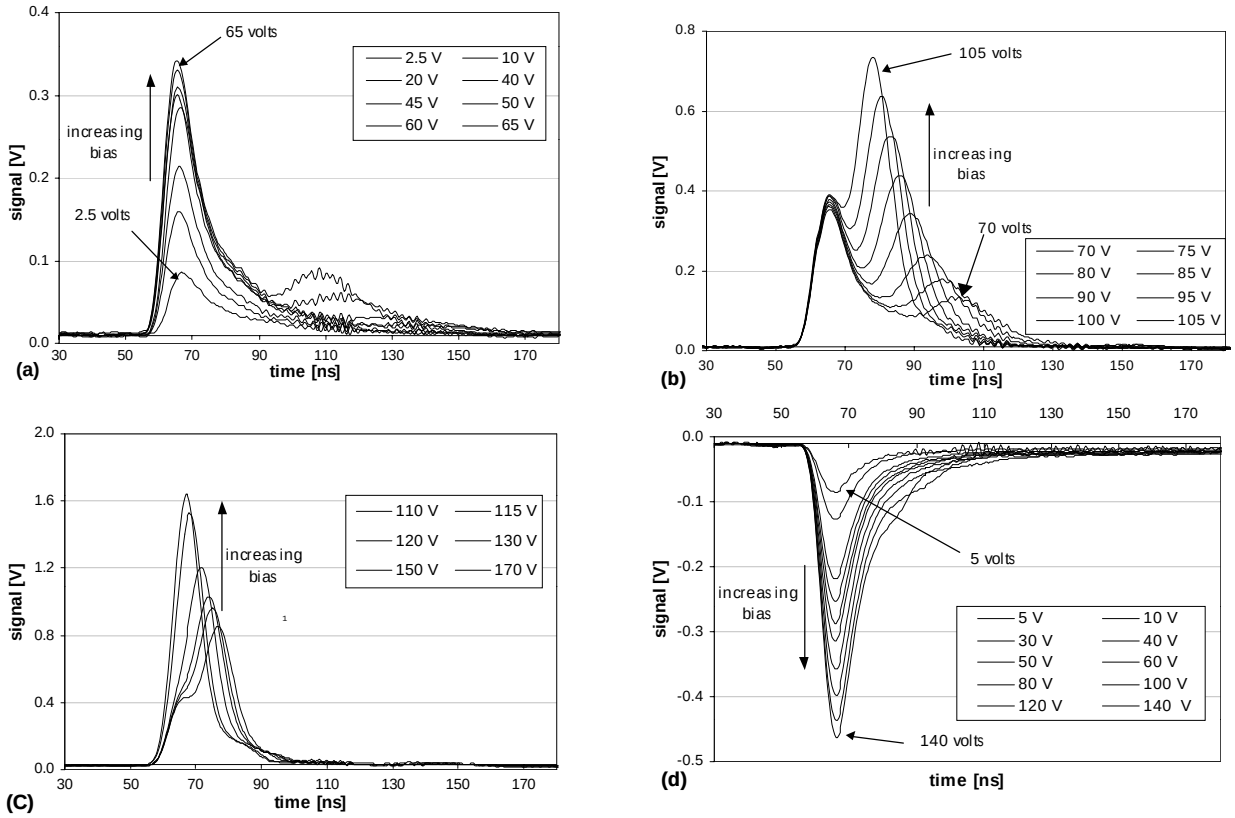

Fig. 7.16 *Signal pulses for 1.7·10^{14} cm^{-2} irradiated diode illuminated by red LED light.*
(a) Front illumination: 2.5-65 V (b) Front illumination: 70-105 V
(c) Front illumination: 110-170 V (d) Rear illumination 5-140 V. V_{FD} = 115 volts.

$$i(0) = \frac{\mu Q_0 E_0}{w} = \frac{\mu Q_0}{w}\frac{qN_{eff}}{\varepsilon_{Si}} \cdot x = \frac{\mu Q_0}{w}\sqrt{\frac{2qN_{eff}}{\varepsilon_{Si}}} \cdot \sqrt{V} \qquad (7.7)$$

where E_0 is the maximum value of the electric field at the junction and x is the depletion depth. Figures 7.12(b), 7.13(b) and 7.14(b) show the CCE versus $V^{1/2}$ for front illumination of heavily irradiated diodes. The charge collection takes place already at low biases. Figures 7.15(a, b, c), 7.16(a, b, c) and 7.17(a, b, c) show the pulse shape for different bias voltages in the case of front illumination for increasing fluences after type inversion. A pulse appears from low biases, well below V_{FD}. The peaking time of this pulse is ≈ 12 ns and it does not evolve with bias, indicating that the charge is moving in a decreasing electric field. This fact excludes that the signal could be induced by the diffusion of charge carriers through the non-depleted bulk and indicates the presence of a sensitive layer and an electric field next to the p^+ contact. This situation can be regarded as a double junction in inverted irradiated detectors.

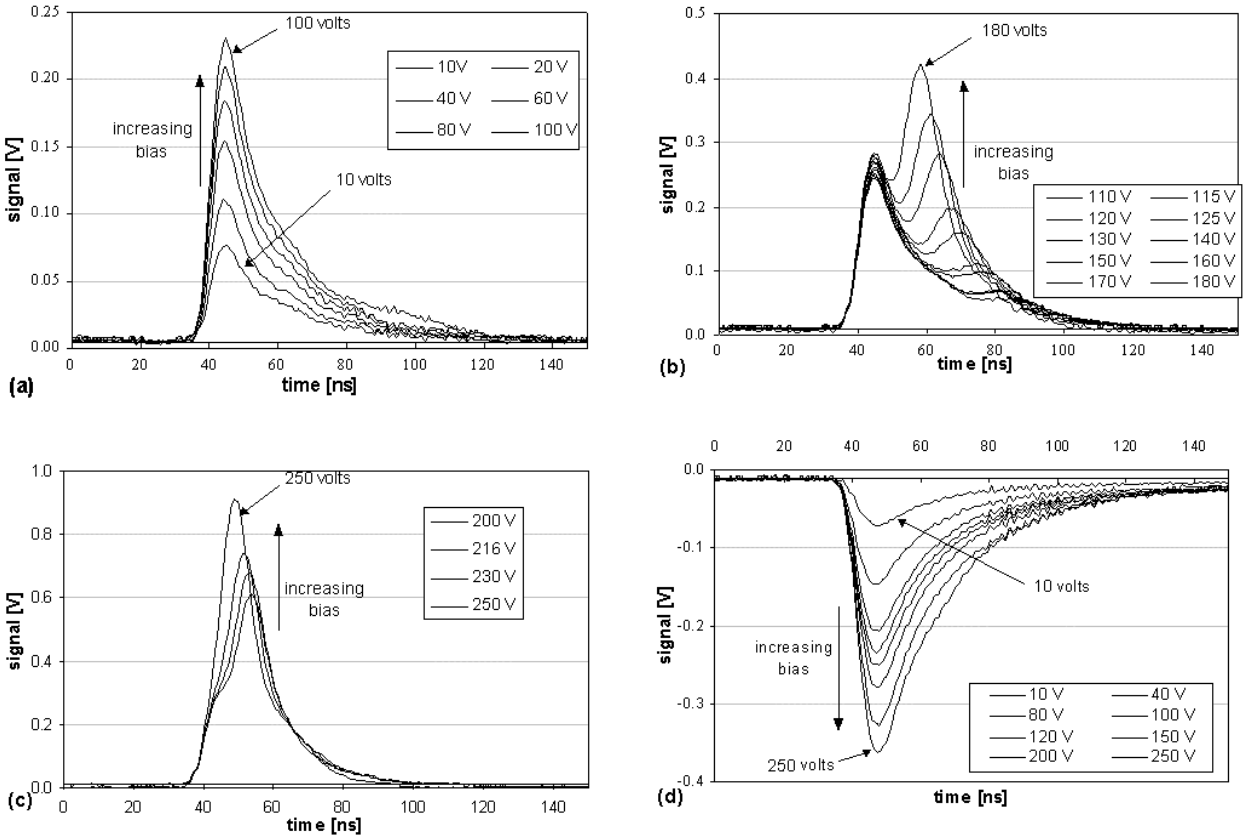

Fig. 7.17 *Signal pulses for $2.9 \cdot 10^{14}$ cm^{-2} irradiated diode illuminated by red LED light.*
(a) Front illumination: 10-100 V (b) Front illumination: 110-180 V
(c) Front illumination: 200-250 V (d) Rear illumination 10-250 V. V_{FD} = 225 volts.

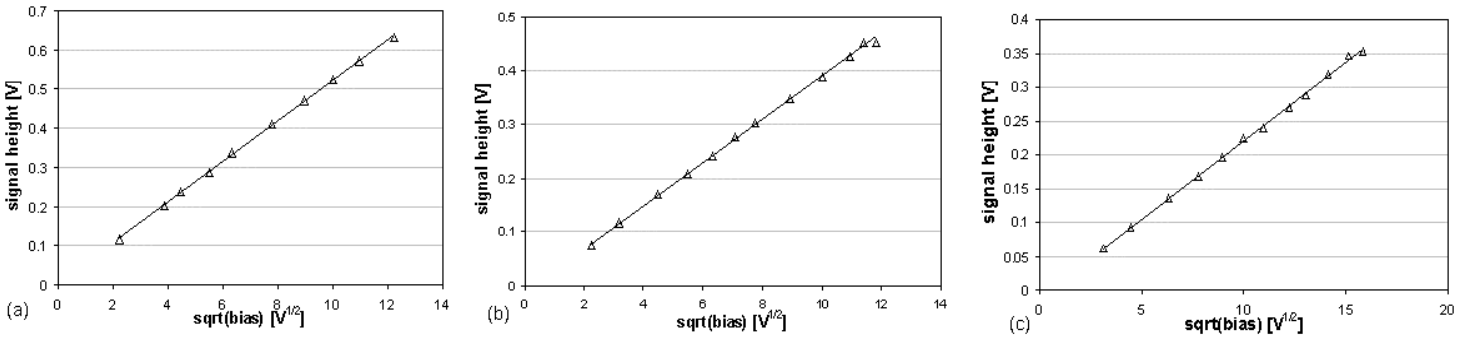

Fig. 7.18 *Height of the signal pulse as a function of $V^{1/2}$ for diodes irradiated up to:*
(a) $1.1 \cdot 10^{14}$ (b) $1.7 \cdot 10^{14}$ and (c) $2.9 \cdot 10^{14}$ cm^{-2}.

A second peak appears when the bias is ≈ 35, ≈ 50 and ≈ 100 volts for the detectors irradiated to the fluence of $1 \cdot 10^{14}$, $1.7 \cdot 10^{14}$ and $2.9 \cdot 10^{14}$ cm^{-2} respectively. The two peaks are well separated at the beginning. Increasing the bias, the peaking time of the second peak (t_{pf})

decreases and the amount of charge carried by it increases. Eventually, the second peak becomes predominant and the two peaks cannot be separated any more.

These experimental results can be explained with the hypothesis of a depleted region on each side of the detector and with an electric field distribution qualitatively shown by Fig. 7.19 as proposed by the Lancaster group [7.3]. A weak electric field should be able to drive the charge in the non-depleted volume between the two depleted regions. The movement of the charge (electrons) in the depleted region next to the front side junction, in the direction of a decreasing field, generates the first peak. The electrons, crossing the intermediate QNB, undergo to a trapping process. When the non-depleted volume narrows enough to permit the electrons to reach the depleted volume next to the main rear side junction, the surviving electrons move in the sensitive volume up to the n^+ contact, inducing the second peak signal.

t_{pf} seems to decrease proportionally to $V^{1/2}$ for bias voltages lower then V_{FD}, as shown by Fig. 7.20. This effect is due mainly to the time to cross the QNB. Below full depletion, t_{pf} can be expressed by:

$$t_{pf} = t_{FD} + \frac{1}{v}(w - x) = t_{FD} + \frac{w}{v}\left(1 - \frac{\sqrt{V}}{\sqrt{V_{FD}}}\right) \tag{7.8}$$

where t_{FD} is the peaking time at full depletion, v the velocity of the carriers in the QNB, w the detector thickness and x the depleted volume depth. The fit of the experimental data with eq. 7.8 allows the evaluation of the velocity. The strength of the electric field in the non-depleted bulk, E_0, is calculated using $E_0 = v/\mu$. The mobility value, μ, used here is 1100 V^{-1} cm^2 s^{-1} [7.4]. The values of v and E_0 are reported in Table 7.2 for three different irradiation levels.

Fluence [cm^{-2}]	**Velocity [cm s^{-1}]**	**E_0 [V cm^{-1}]**
$1 \cdot 10^{14}$	$1.35 \cdot 10^5$	123
$1.7 \cdot 10^{14}$	$1.45 \cdot 10^5$	132
$2.9 \cdot 10^{14}$	$2.31 \cdot 10^5$	210

Table 7.2 *Values of the velocity and of the electric field in the quasi-neutral bulk (QNB) bulk.*

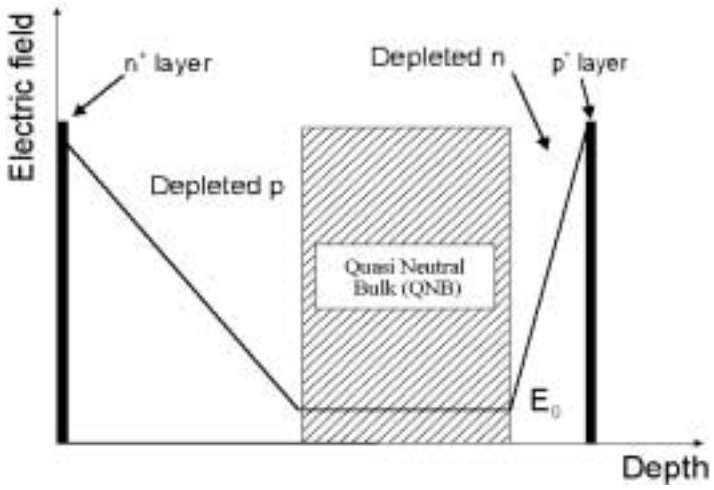

Fig. 7.19 *Qualitative electric field distribution in a detector irradiated above type inversion [7.3].*

The electric field (E) shape shown by Fig. 7.19 is qualitative. The actual E distribution in the QNB is probably not constant and evolves as a function of the bias applied to the detector. If E is proportional to $V^{1/2}$ in the QNB, the expressions for the velocity and for t_{pf} are:

$$v = v_M \left(\frac{V}{V_{FD}} \right)^{\frac{1}{2}} = v_M \left(\frac{x}{w} \right) \tag{7.9}$$

$$t_{pf} = t_{FD} + \frac{1}{v}(w - x) = t_{FD} + \frac{w}{v_M} \left(\sqrt{\frac{V_{FD}}{V}} - 1 \right) \tag{7.10}$$

where v_M is the maximum velocity at full depletion. Figure 7.21 shows t_{pf} as a function of $(V_{FD}/V)^{1/2}$ for three different fluences after inversion. The values of v_M and of the maximum electric field in the QNB (at full depletion) are listed in Table 7.3 for the different fluences.

Fluence [cm^{-2}]	**v_M [cm s^{-1}]**	**E_M [V cm^{-1}]**
$1 \cdot 10^{14}$	$1.74 \cdot 10^{5}$	158
$1.7 \cdot 10^{14}$	$2.44 \cdot 10^{5}$	222
$2.9 \cdot 10^{14}$	$3.5 \cdot 10^{5}$	318

Table 7.3 *Values of the v_M and E_M for three heavily irradiated diodes.*

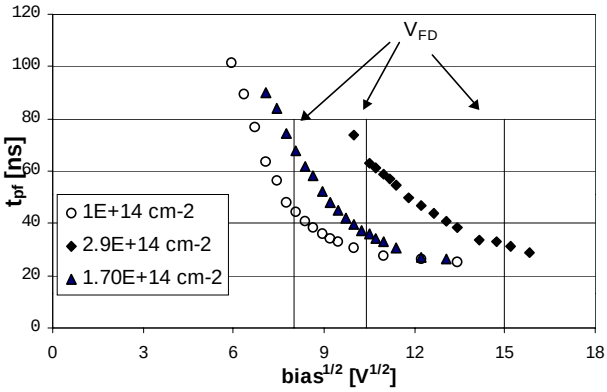

Fig. 7.20 *Peaking time of the second peak (t_{pf}) as a function of $V^{1/2}$ for front illumination of three heavily irradiated diodes.*

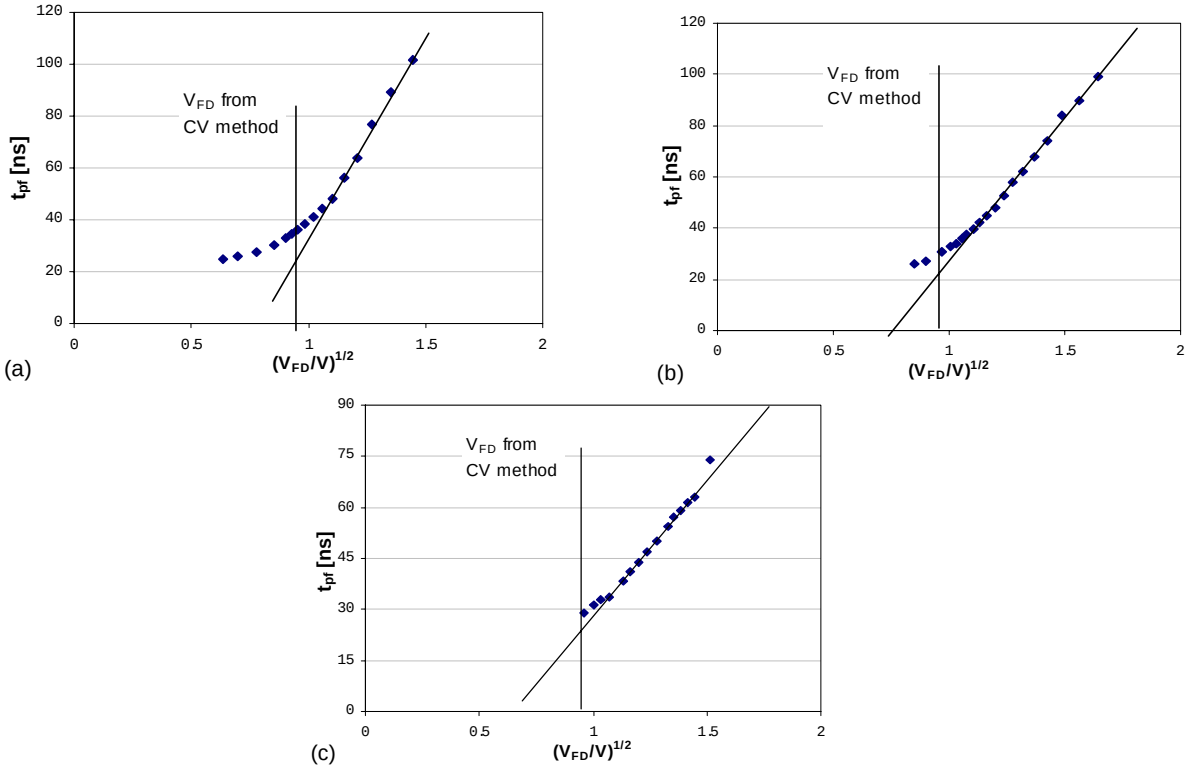

Fig. 7.21 *Peaking time of the second peak (t_{pf}) as a function of $(V/V_{FD})^{1/2}$ for front illumination of three heavily irradiated diodes: (a) $1.1 10^{14}$ cm^{-2} (b)$1.7 10^{14}$ cm^{-2} (c) $2.9 10^{14}$ cm^{-2}.*

For type-inverted detectors the double peak is only visible when the diode is illuminated on the front side. The electric field distribution shown by Fig. 7.19 predicts a double peak also in the case of injection in the rear side. In that case, in a partially depleted detector, the holes generated from the light drift towards the anode in the depleted rear side volume.

The carriers reach the QNB bulk, undergoing to the trapping and the surviving carriers induce a second signal moving in the depleted front-side bulk. The situation is symmetric to the signal induced by electrons for the case of front illumination. The absence of the second peak and the linearity of the CCE as a function of $V^{1/2}$ indicate that the signal due to the holes moving in the front-side depleted bulk is negligible. This can be explained by the more effective trapping of holes in the QNB, due to their lower mobility, and by the smaller depth of the front-side compared to the rear-side depleted region.

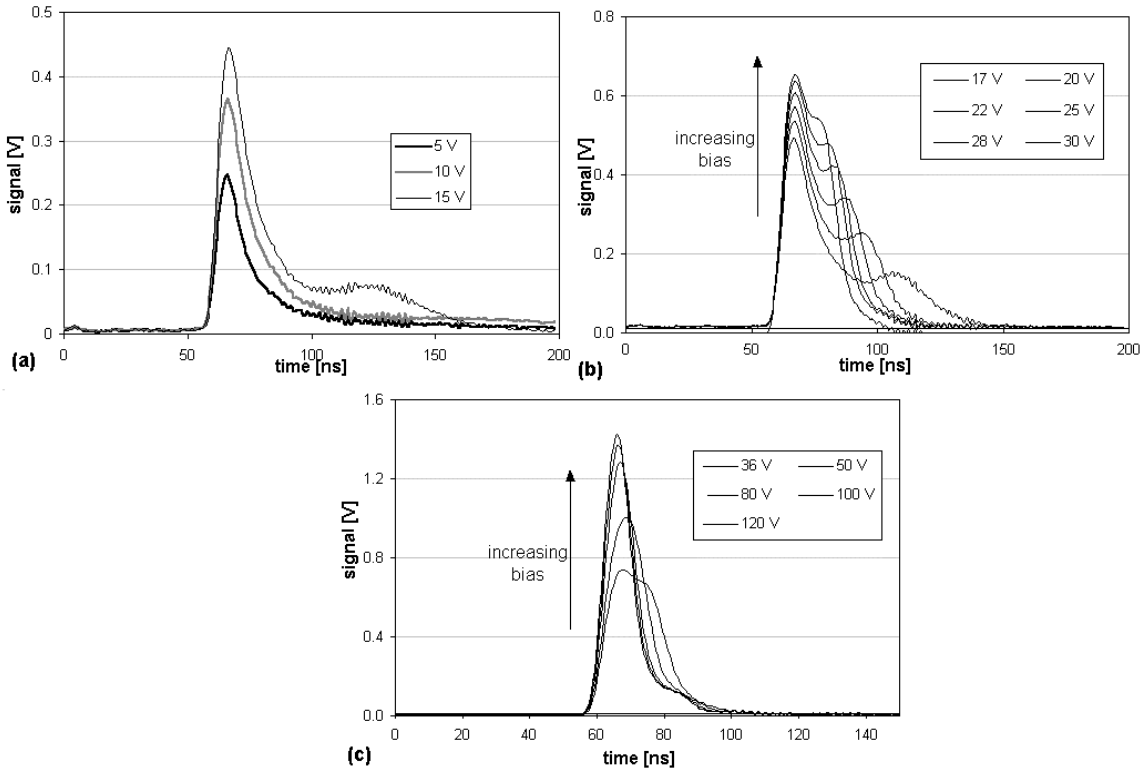

Fig. 7.22 *Signal pulses for front illumination of a 5.3·10^{13} cm^{-2} irradiated diodes (≈ Φ_{inv}): (a) 5-15 V, (b) 17-30 V and (c) 36-120 V.*

For detectors irradiated at a fluence close to the type inversion one, Φ_{inv}, the double-peak of the signal is visible for illumination on both sides. Fig. 7.22 (a)(b)(c) and Fig. 7.23(a)(b)(c) show the signal pulses for the front and rear illumination of a diode irradiated up to 5.2·10^{13} cm^{-2}. The second peak appears in both cases at ≈ 15 volts. Figure 7.24 shows the peaking time as a function of $V^{1/2}$ for front and rear illumination of this diode. The different mobility of electrons and holes explains the different values of t_p measured in the case of front and rear illumination.

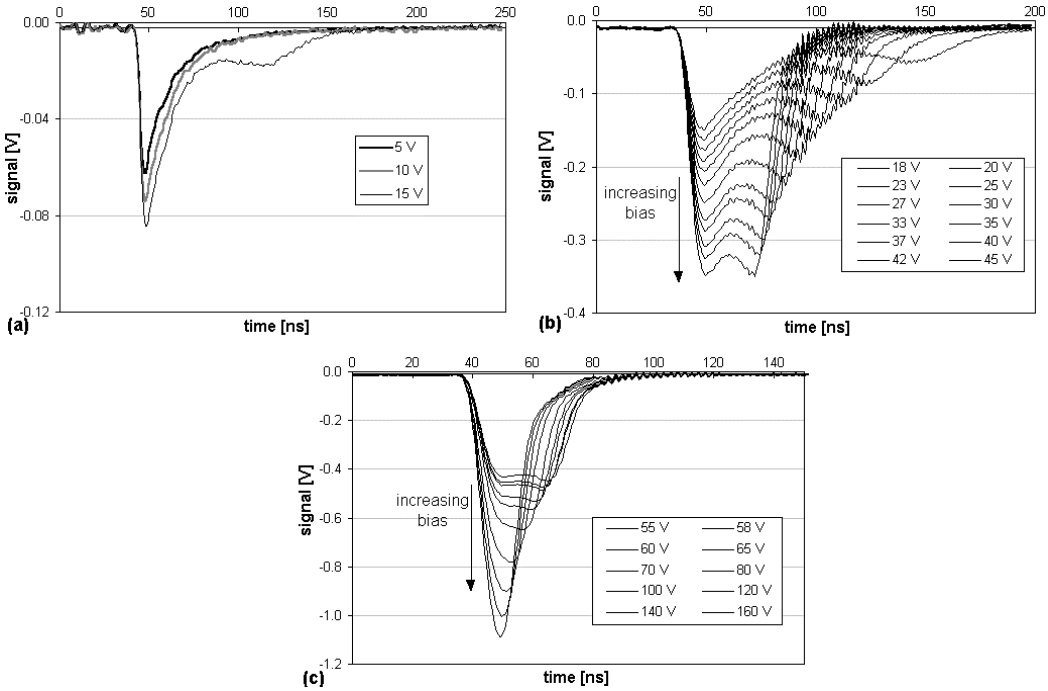

Fig. 7.23 *Signal pulses for rear illumination of a 5.3·10^{13} cm^{-2} irradiated diodes (≈ Φ_{inv}): (a) 5-15 V, (b) 18-45 V and (c) 55-160 V.*

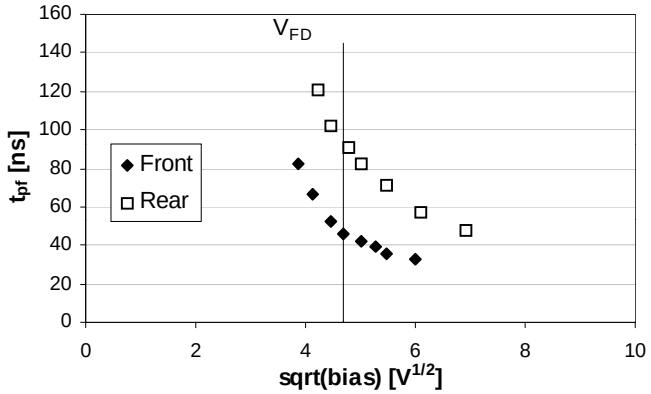

Fig. 7.24 *Peaking time of the second peak (t_{pf}) as a function of $(V/V_{FD})^{1/2}$ for front and rear Illumination of a diode irradiated up to 5.210^{13} cm^{-2}.*

The charge collection efficiency curves as a function of $V^{1/2}$ for front illumination of inverted diodes (Fig. 7.12(b), 7.13(b) and 7.14(b)) can be divided in three parts. At lower biases there is a linear dependence on $V^{1/2}$ due to the contribution of the first peak only. By increasing the bias, the contribution of the first peak to the collected charge saturates. The second peak

develops and contributes to the collected charge. The contribution of this peak is not linear on $V^{1/2}$ because of the trapping suffered by the charge traversing the QNB bulk. The CCE as a function of the bias in the interval from the appearance of the second peak contribution, V_S, to V_{FD} can be expressed by:

$$CCE = C_1 + C_2\sqrt{V}\,e^{-\frac{y}{a}} \tag{7.11}$$

where

$$y = w - d = w\left(1 - \frac{\sqrt{V}}{\sqrt{V}_{FD}}\right) \tag{7.12}$$

is the thickness of the non-depleted bulk and a is the attenuation length of electrons. The constant C_1 and C_2 can be found using the boundary conditions $CCE = C_S$ for $V = V_S$ and $CCE = Q_{FD}/Q_M = exp(-t_{FD}/\tau_{tr})$ for $V = V_{FD}$, where Q_M is the maximum collected charge. Q_{FD}/Q_M, C_S and V_S are experimentally evaluated for any fluence. The expression for C_1 and C_2 are then

$$C_1 = E_{FD} - C_2\sqrt{V_{FD}} \tag{7.13}$$

$$C_2 = \frac{(E_{FD} - C_S)}{\sqrt{V_{FD}}\left(1 - ye^{-\frac{w}{a}(1-\xi)}\right)} \tag{7.14}$$

where $\xi = \sqrt{V_S / V_{FD}}$. The value of a, which defines the attenuation length of the electrons in the QNB bulk, is between 70 to 90 µm for the heavily irradiated diodes, as obtained from the fits of the CCE curves shown by Fig. 7.12(b), 7.13(b) and 7.14(b).

Evaluation of N_{eff} from charge collection curves

N_{eff} can be estimated from the fit of the CCE as a function of $V^{1/2}$ using eq. 7.1. Table 7.4 lists the values of N_{eff} obtained by fitting the CCE curves of heavily irradiated diodes as compared to the values obtained from the double line interpolation technique applied to the C-V characteristics. The differences between the values obtained by the two methods arise from the uncertainty on the value from the amount of trapping in the case of the CCE method and from the error due to the adjustment of the interpolating lines on the C-V curve, as discussed in § 4.1. The two methods agree rather well.

Irradiation fluence [cm^{-2}]	N_{eff} (C-V method) [cm^{-3}]	N_{eff} (CCE method) [cm^{-3}]
$1.1 \cdot 10^{14}$	$1.5 \cdot 10^{12}$	$1.7 \cdot 10^{12}$
$1.7 \cdot 10^{14}$	$1.9 \cdot 10^{12}$	$2.3 \cdot 10^{12}$
$2.9 \cdot 10^{14}$	$3.8 \cdot 10^{12}$	$3.7 \cdot 10^{12}$

Table 7.4 *Comparison between N_{eff} for three heavily irradiated diodes calculated using the C-V and the CCE methods.*

7.3 Discussion

The data presented in the previous sections show that the changes of the charge collection properties of irradiated silicon detectors are correlated to the changes in the quasi neutral bulk, QNB. The high density of radiation induced defects leads to a very low level of free carriers. This argument has already been used to explain the independence of the capacitance on the bias for high frequency C-V measuring signal [§ 4.1].

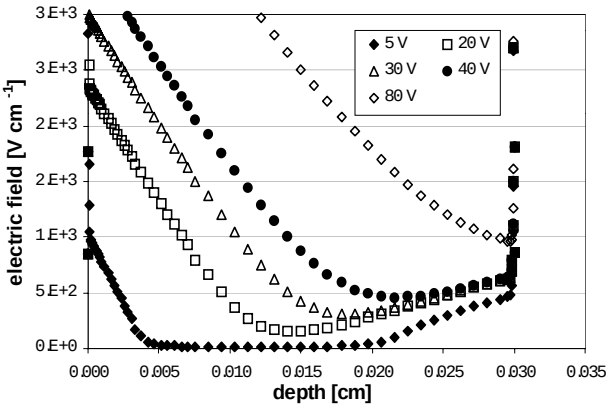

Fig. 7.25 *Simulated [7.7] electric field distribution versus depth for heavily irradiated detectors at different values of the applied bias.*

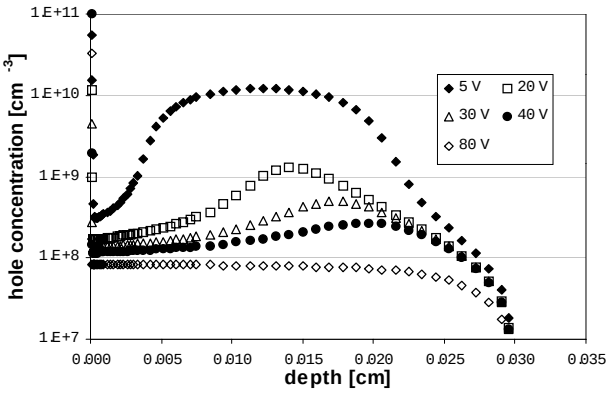

Fig. 7.26 *Concentration of free majority carriers (holes) as a function of depth for heavily irradiated detectors at different values of the applied bias.*

The low density of carriers is compatible with a weak electric field in the QNB. The charge

collection behaviours for shallow ionisation show the presence of a high electric field on both sides of irradiated detectors. For heavily irradiated diodes, the velocity of charge carriers inside the QNB between the high field regions next to the electrodes is more than 10 times larger than the velocity for non-irradiated detectors. This is explained by the presence of a weak electric field (E_{QNB}) in the QNB. This electric field is found to increase with fluence.

The shape of E_{QNB} shown by Fig. 7.19 is qualitative. The actual distribution must be calculated solving the Poisson equation for the irradiated detectors. Figure 7.25 shows the simulation of the electric field distribution and Fig. 7.26 the free carrier density as a function of the bias for heavily irradiated diodes, performed by the Perugia group [7.5] [7.6]. It can be observed a low free carrier density and a weak electric field inside the QNB already at low biases. E_{QNB} is not constant inside the QNB. Figure 7.27 shows another example of the simulated values of the electric field at 100, 150 and 200 µm depths as a function of $V^{1/2}$ [7.7]. Actually, its trend is proportional to $V^{1/2}$, indicating that the dependence of t_p on the applied bias as expressed by eq. 7.10 is more correct. The simulations are based on the hypothesis that the radiation-induced defects are acceptors and donors, with energy levels in the bandgap of E_C - 0.50 and E_V + 0.36 for the acceptor and the donor defects, respectively [7.8].

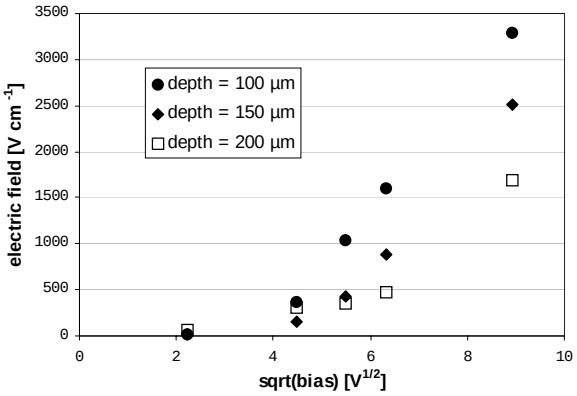

Fig. 7.27 *Simulated values [7.6] of the electric field at 100, 150 and 200 µm depths as a function of $V^{1/2}$.*

The above discussion shows that n-type diodes irradiated above the type inversion fluence cannot be modelled as simple p-type diodes. Moreover, the concept of depletion seems to be inadequate to describe inverted silicon diodes. The presence of E_{QNB} implies a low density of

free carriers in the QNB already at biases noticeably lower than V_{FD}, as measured by the CV method or evaluated by the CCE curves. V_{FD} should correspond, in this model, to the voltage at which the depth of QNB is zero and the E_{QNB} disappears.